Title

FoxO4 interacts with the sterol regulatory factor SREBP2 and the hypoxia inducible factor HIF2α at the CYP51 promoter

Journal

Journal of Lipid Research, 55(3)

ISSN

0022-2275

Authors

Zhu, Jun
Jiang, Xiangning
Chehab, Farid F

Publication Date

2014-03-01

DOI

10.1194/jlr.m043521

Peer reviewed

FoxO4 interacts with the sterol regulatory factor SREBP2 and the hypoxia inducible factor HIF2α at the CYP51 promoter

Jun Zhu,* Xiangning Jiang,† and Farid F. Chehab[1,*]

Departments of Laboratory Medicine* and Pediatrics,† University of California, San Francisco, CA 94143

Abstract The late steps of cholesterol biosynthesis are oxygen demanding, requiring eleven oxygen molecules per synthesized cholesterol molecule. A key enzymatic reaction, which occurs at the top of the Bloch and Kandutsch-Russell pathways, is the demethylation of lanosterol and dihydrolanosterol (DHL). This reaction is catalyzed by lanosterol 14α demethylase (CYP51) and requires three oxygen molecules. Thus, it is the first step in the distal pathway to be susceptible to oxygen deprivation. Having previously identified that the forkhead transcription factor 4 (FoxO4) represses CYP51 expression, we aimed to characterize its role at the CYP51 promoter. Hypoxia-treated 3T3L1 cells showed decreased cholesterol biosynthesis, accumulation of lanosterol/DHL, and stimulation of FoxO4 expression and its cytoplasmic translocation to the nucleus. Transfection assays with a CYP51 promoter reporter gene revealed that FoxO4 and sterol regulatory element binding protein (SREBP)2 exert a stimulatory effect, whereas FoxO4 and the hypoxia inducible factor (HIF)2α repress CYP51 promoter activity. Electromobility shift, chromatin immunoprecipitation, pull-down, and coimmunoprecipitation assays show that FoxO4 interacts with SREBP2 and HIF2α to modulate CYP51 promoter activity. We also show an inverse correlation between FoxO4 and CYP51 in adipose tissue of ob/ob mice and mouse fetal cortical neurons exposed to hypoxia. Overall, these studies demonstrate a role for FoxO4 in the regulation of CYP51 expression.—Zhu, J., X. Jiang, and F. F. Chehab. **FoxO4 interacts with the sterol regulatory factor SREBP2 and the hypoxia inducible factor HIF2α at the CYP51 promoter. *J. Lipid Res*. 2014.** 55: **431–442.**

Supplementary key words cholesterol • dihydrolanosterol • lanosterol 14α demethylase • forkhead transcription factor 4 • hypoxia-inducible factor 2α • sterol regulatory element binding protein 2

The late steps of cholesterol biosynthesis encompass a series of demethylation, reduction, and desaturation enzymatic reactions that involve multiple sterol intermediates. A key enzymatic reaction that occurs at the top of this distant pathway is the demethylation of lanosterol at C14 by sterol 14α demethylase, also known as CYP51 (1). This reaction occurs either directly after lanosterol biosynthesis or following its reduction to dihydrolanosterol (DHL) by sterol 24-reductase (DHCR24) in the Bloch or Kandutsch-Russell arms of the distal pathway, respectively (**Fig. 1**). While the proximal pathway, also referred to as the early steps of cholesterol biosynthesis, requires a single oxygen molecule for the conversion of squalene to lanosterol, the distal pathway consumes 10 additional oxygen molecules, three of which are required for the lanosterol 14α demethylation step. Thus, this oxidative step is most sensitive to reduced oxygen availability and is likely to be coupled in hypoxic states with regulatory mechanisms that conserve oxygen to ensure cell survival. It has long been known that compounds from the triazole family, such as itraconazole, miconazole, ketoconazole, and their derivatives, inhibit cholesterol synthesis by interfering with the activity of CYP51, resulting in the accumulation of lanosterol and DHL. More recently, hypoxia was shown to result in ubiquitin-mediated degradation of HMG-CoA reductase (HMGCR) and accumulation of lanosterol and DHL (2). We have previously shown that overexpression of the forkhead transcription factor 4 (FoxO4) in mouse 3T3L1 cells is associated with a significant reduction of CYP51 mRNA, resulting in the accumulation of DHL (3). However, the

This work was supported by grants from the University of California, San Francisco (UCSF) Academic Senate, National Institutes of Health (NIH)/UCSF Diabetes Center Grant P30 DK063720, and NIH Grant T32 DK07636. Instrument acquisition and method development at the Kansas Lipidomics Research Center was supported by National Science Foundation Grants MCB 0455318, MCB 0920663, DBI 0521587, DBI 1228622, Kansas IDeA Network of Biomedical Research Excellence (INBRE) (NIH Grant P20 RR16475 from the INBRE program of the National Center for Research Resources), NSF EPSCoR Grant EPS-0236913, Kansas Technology Enterprise Corporation, and Kansas State University.

Manuscript received 30 August 2013 and in revised form 4 December 2013.

Published, JLR Papers in Press, December 18, 2013
DOI 10.1194/jlr.M043521

Abbreviations: ARNT, aryl hydrocarbon receptor nuclear translocator; ChIP, chromatin immunoprecipitation; CYC, cyclophilin A; CYP51, lanosterol 14α demethylase; DBE, Daf-16 binding element; DHCR24, dihydrocholesterol reductase 24; DHL, dihydrolanosterol; EMSA, electromobility shift assay; FoxO4, forkhead transcription factor 4; HA, hemagglutinin; HIF, hypoxia inducible factor; HMGCR, HMG-CoA reductase; HMGCS, HMG-CoA synthase; HRE, hypoxia responsive element; nSREBP, mature nuclear form of sterol regulatory element binding protein; SRE, sterol regulatory element; SREBP, sterol regulatory element binding protein; WAT, white adipose tissue.

[1] To whom correspondence should be addressed.
e-mail: chehabf@labmed2.ucsf.edu.

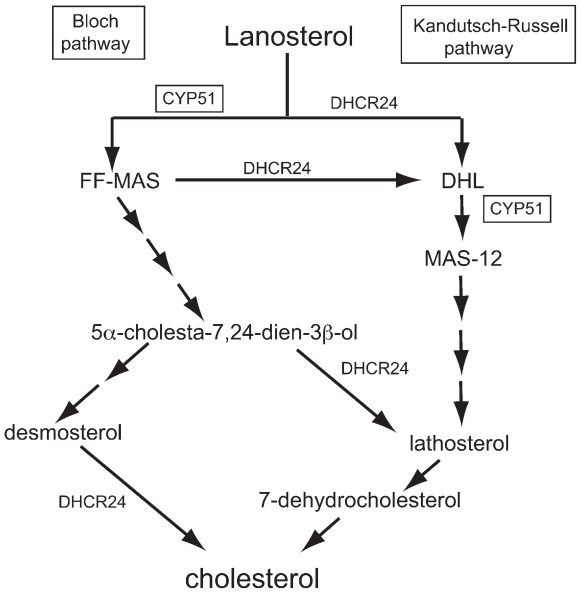

Fig. 1. Condensed diagram for the distant cholesterol biosynthesis pathway showing the CYP51 enzymatic step, which can occur either immediately after lanosterol synthesis in the Bloch arm of the pathway or following reduction of lanosterol at C24 by dihydrocholesterol reductase 24 (DHCR24) in the Kandutsch-Russell arm of the pathway.

underlying mechanism for this repression is unknown. Thus, we undertook to uncover the transcriptional factors and cofactors that mediate CYP51 repression. We show in this study that FoxO4 interacts with the mature nuclear form of sterol regulatory element binding protein (nSREBP)2 and hypoxia inducible factor (HIF)2α, singly or in combination, to regulate CYP51 expression.

MATERIALS AND METHODS

Hypoxia treatment

Cells were plated in 6-well plates and grown in DMEM supplemented with 10% fetal calf serum (FCS). Mouse 3T3L1 cells were maintained in normoxia under ambient conditions at 37°C, 5% CO_2, in a humidified incubator. For hypoxia treatment, cells seeded in 6-well plates were placed in a Billups-Rothenberg chamber, which was flushed for 5 min with 1% O_2 and 99% N_2, then sealed and incubated for 24 h at 37°C.

Lipid extraction and thin-layer chromatography

De novo lipid biosynthesis was determined with the incorporation of ^{14}C-acetate (57 mCi/mmol, 0.2 μCi/μl) in 3T3L1 cells fed DMEM and 10% FCS. Lipid extraction, fractionation, thin-layer chromatography (TLC), autoradiography, and protein assays were performed as previously described (3, 4).

GC/MS

Lipid extracts were saponified, derivatized with trimethylchlorosilane, dried under nitrogen, and dissolved in 100 μl hexane. Two microliters were then used for subsequent analysis. GC/MS was performed on an Agilent 6890N gas chromatograph coupled to an Agilent 5975N quadrupole mass selective detector. The gas chromatograph was fitted with a DB-5MS capillary column with a 5% phenyl methyl siloxane stationary phase (column length, 60 mm; internal diameter, 250 μm; film thickness, 0.25 μm). Helium was used as the carrier gas at a column flow rate of 1 ml/min. The front inlet was operated at a pressure of 19.35 psi and 280°C. The Agilent 7683 autosampler was used to inject 2 μl of the sample in the splitless mode. The gas chromatograph temperature program was: initial temperature of 80°C, 25°C/min to 300°C at 3°C/min to a final temperature of 325°C, held for 5 min. The mass spectrometer was operated in the electron impact mode at 70 eV ionization energy. The mass spectrometer quad temperature was 150°C and the source temperature was 230°C. The data acquisition was in scan mode with a scan mass of 50 to 650. The data were processed with Agilent Chemstation software and normalized to the protein content of each lipid extract. Data were analyzed by two-tailed *t*-test with a *P* value set at <0.01.

Realtime PCR

3T3L1 cells were treated with normoxia (n = 6 wells) and hypoxia (n = 6 wells) as described above. RNA was extracted with the Trizol reagent. Five micrograms of RNA from each well were reverse transcribed into cDNA and equal aliquots subjected to quantitative (q)PCR using a SybrGreen Qiagen fluorescent PCR mix. DHCR24, CYP51, FoxO4, and cyclophilin A (CYC) mRNA expressions were determined in triplicate for each well with the PCR primers listed in **Table 1**. Melting curves for each amplicon were verified after amplification to ensure integrity of the amplification product. CYC was simultaneously amplified as an internal control to provide normalization of the data. Cycle threshold values were analyzed with the QGene software based on each amplicon's amplification efficiency, which was derived from their respective standard curves. Data were analyzed by two-tailed *t*-test with a *P* value set at <0.01.

Expression and cellular localization of HA-FoxO4 following hypoxia

Protein lysates extracted from normoxia- and hypoxia-treated confluent 3T3L1 cells were used to prepare Western blots that were probed with anti-mouse HIF1α (Novus Biologicals, Littleton, CO) and anti-mouse HIF2α (Cell Signaling, Danvers, MA). FoxO4 mRNA expression was determined by qPCR from 3T3L1 cells exposed to normoxia and hypoxia as described above. Hemaglutinin-tagged FoxO4 (HA-FoxO4) overexpressing 3T3L1 cells were grown on cover slips and treated overnight with hypoxia. Cover slips were fixed in ice-cold acetone, blocked with 10% newborn calf serum for 1 h, washed, and conjugated with anti-HA for 2 h at room temperature. Detection was performed with FITC-conjugated secondary anti-rabbit for 1 h at room temperature followed by visualization with fluorescence microscopy. DAPI was used as a control for nuclei staining. Cytoplasmic and

TABLE 1. PCR primers (5′ to 3′) used for realtime PCR

	Forward	Reverse
DHCR24	GCTGCGAGTCGGAAAGTACAAGAA	TGTCACCTGACCCATAGACACCAA
CYP51	ACGCAGACCTGGATGGAGGTTTTA	TCTTTTGACAGCCTGCGCTTC
FoxO4	TCATCAAGGTTCACAACGAGGC	AGGACAGACGGCTTCTTCTTGG
CYC	CCATCCAGCCATTCAGTCTTGG	AGGACAGACGGCTTCTTCTTGG

nuclear extracts were prepared with a nuclear extraction kit from Active Motif (Carlsbad, CA).

Expression constructs

The mouse CYP51 promoter was amplified with the primers 5′-GGTGCTTGCAGTTTTGCCAATCACTGC-3′ and 5′-TGGCGGAGGGATCTCAGGACCAGATTG-3′, yielding a 627 bp amplicon that was subcloned in pcDNA 3.1 TOPO (Invitrogen). The insert was recovered as a *Hind*III/*Xho*I fragment and subcloned in the luciferase vector pGL3. A full-length human SREBP2 cDNA clone was obtained from Origene (Rockville, MD) in the plasmid pCMV6-XL4 and its mature nuclear form (nSREBP2) (extending from amino acid 2 to amino acid 468) was amplified by PCR and subcloned into the expression vector pcDNA3.1D-V5-HIS. The resulting clone carried the V5 tag for antibody detection and the 6x histidine tag for protein purification and pull-down assays with the nickel nitrilotriacetic acid (Ni-NTA) resin. Plasmids containing HA-tagged human HIF1α and HIF2α (5, 6) and human FLAG-FoxO4 were purchased from Addgene as plasmids 18949, 18950, and 17549, respectively. Mouse FoxO4-3xHA and human HA-FoxO4 were kind gifts from Karen Arden (University of California, San Diego) and Boudjewin Burgering (University of Utrecht), respectively. All constructs were verified by Sanger dideoxy DNA sequencing.

Transfection and luciferase assays

All transient transfection assays were conducted in HEK293 cells that are efficient in uptaking exogenous DNA. HEK293 cells were maintained in DMEM and 10% serum at 37°C in a 5% CO_2 humidified incubator. Plasmid DNA was prepared and transfected into near confluent HEK293 cells plated 24 h prior to transfection in 6-well plates. Transfections were performed with the lipid-based transfection reagent Superfect (Stratagene) in triplicate wells and consisted each of 0.4 μg plasmid DNA of the CYP51 promoter luciferase construct, 0.03 μg DNA of Renilla luciferase plasmid, and 0.15 μg plasmid DNA of each nSREBP2, HIF1α, HIF2α, and FoxO4 in various combinations. Negative controls consisted of HEK293 cells transfected with only the CYP51 promoter luciferase construct without any added nSREBP2, FoxO4, or HIF2α plasmid DNA. Dual Firefly and Renilla luciferase activities were determined 24 h post transfection with the Dual-Glo reagent (Invitrogen) using a luminometer (Turner Designs). The average of the triplicates of each transfection well was calculated as a measure of reporter gene expression.

Recombinant protein purification and in vitro translation

The full-length open reading frames of FoxO4 and nSREBP2 were each cloned in the bacterial expression vector pQE81 in frame with the 6x histidine tag. The full-length HIF2α open reading frame was excised from Addgene plasmid 189950 and cloned in frame with the 6x histidine tag in pQE80. Recombinant proteins were expressed in *Escherichia coli*, purified from bacterial lysates by affinity chromatography using Ni-NTA columns and refolded by step-dialysis against phosphate-buffered saline (PBS) as previously described (7). HIF2α was translated from an expression plasmid with the TNT system (Promega) and T7 RNA polymerase.

Electromobility shift assays

Double-stranded DNA probes were prepared by annealing 2 μg each of two complementary oligonucleotide probes (**Table 2**) at room temperature for 30 min in annealing buffer [20 mM HEPES (pH 7.9), 20 mM KCl, 4 mM $MgCl_2$, 1 mM EDTA, 4% glycerol]. The double-stranded annealed products were then gel purified following electrophoresis on 2% agarose gels. Double-stranded probe (100 ng) was labeled for 30 min with 10 μCi of ^{32}P-γ-ATP using T4 polynucleotide kinase, then purified by spin-column chromatography and an aliquot counted for incorporated radioactivity. Specific activities were approximately 4 × 10^7 CPM/μg. All electromobility shift assay (EMSA) reactions were carried out in 20 μl of annealing buffer and contained approximately 100,000 CPM probe, 0.1 mM dithiothreitol, 20 ng poly(dI-dC) (Sigma), recombinant proteins, TNT lysates, competing probes, and antibodies. Supershift antibodies were anti-HA (Cell Signaling), anti-HIF2α (Novus), anti-aryl hydrocarbon receptor nuclear translocator (ARNT) (Novus), and mouse and rabbit IgG (Upstate). Reactions were incubated for 20 min at 25°C before fractionation on 5% polyacrylamide gels (20 × 20 cm) and were run at 120 V for 4–6 h at 4°C in 0.5× Tris-borate buffer.

Chromatin immunoprecipitation

3T3L1 cells overexpressing HA-FoxO4 were grown to confluence in 10 cm dishes in DMEM and 10% serum. Cells were treated at room temperature with 37% formaldehyde for 15 min and 2.5 M glycine for 5 min. Cells were then washed with PBS, scraped off the dish, and processed for chromatin preparation. We used the Simple-ChIP chromatin immunoprecipitation kit (catalog number 003) from Cell Signaling (Beverly, MA) using the manufacturer's recommendations. Chromatin immunoprecipitation (ChIP) of HA-FoxO4 and HIF2α was performed with anti-HA (Cell Signaling), anti-FoxO4 (Santa Cruz), or anti-HIF2α (Novus). For a negative ChIP control, we used mouse IgG (Upstate). Following ChIP, the bound DNA was released, ethanol precipitated, and dissolved in 50 μl 10 mM Tris (pH 8.0). The hypoxia responsive element (HRE) and Daf-16 binding element (DBE) regions of the CYP51 promoter were amplified by PCR from a 5% chromatin input control and a 2 μl aliquot of the immunoprecipitated DNA. PCR primers for DBE and HRE amplified 150 bp and 282 bp, respectively, and consisted of 5′-AGAACAGGAGTTTGGGGACA-3′, 5′-CCCGTACAATCTGCTTGACA-3′, and 5′-CAGCAGCACACCAAACAACT3′, 5′AGGTGATCTCGCCTATGTG-3′. The PCR products were finally run on a 2% agarose gel and stained with ethidium bromide.

TABLE 2. Oligonucleotide sequences (5′ to 3′) for the double-stranded probes used in the electromobility shift assays

	(+) Strand	(−) Strand
SRE	CATAGGCCGAGATCACCTCAGCAGC	GCTGCTGAGGTGATCTCGGCCTATG
mSRE	CATAGGCCGAGTTTTTTTTTTCAGC	GCTGAAAAAAAAAACTCGGCCTATG
DBE	TATGGCCTGTATTTATTTTAAAAGA	TCTTTTAAAATAAATACAGGCCATA
mDBE	TATGGCCTGCCCCCCCTTTAAAAGA	TCTTTTAAAGGGGGGGCAGGCCATA
HRE	CAGCAGCGCGTGGTGCAATCACAG	CTGTGATTGCACCACGCGCTGCTG
mHRE	CAGCAGCTTTTTGTGCAATCACAG	CTGTGATTGCACAAAAAGCTGCTG

The DNA binding motifs of each transcription factor are underlined.

Pull-down assays, ChiP, and Western blotting

Plasmids were transfected in HEK293 cells using the Superfect or Lipofectamine reagents according to the conditions specified by the manufacturers. Forty-eight hours later, cells were harvested and protein extracts prepared in RIPA buffer. Extracts were bound overnight at 4°C to either Ni-NTA beads for pull-down assays or a specific antibody for ChIP. Antibodies for ChIP and Western blotting were: anti-HA, anti-FoxO4 (Santa Cruz), or anti-V5. Western blotting was performed using 1:1,000 and 1:3,000 dilutions for primary and secondary antibodies, respectively. Chemiluminescent detections were performed with the ECL+ reagent (Amersham). Film exposures were approximately for 1 min.

RNA extraction from white adipose tissue of ob/ob mice

All experiments involving mice were reviewed and approved by the UCSF Institutional Animal Care and Use Committee. Visceral white adipose tissue (WAT) was harvested from homozygous normal C57BL/6J and ob/ob female mice weighing 18.1 ± 1.6 g versus 44.5 ± 2.3 g (n = 6 each group) at 8 weeks of age. The tissues were frozen immediately in liquid nitrogen. Total RNA was then extracted from WAT with the Trizol reagent, reverse transcribed, and the resulting cDNA used in qPCR assays.

Hypoxia treatment of cortical mouse neurons

Primary cortical neurons were prepared from the brains of embryonic day 16 C57BL/6J mice as previously described (8) and subjected to hypoxia 7 days later in a Billups-Rothenberg chamber flushed with of 95% N_2/5% CO_2 for 3 h. Oxygen concentration was maintained at 0.3–0.5% and monitored by an oxygen analyzer (MSA Medical Products, Pittsburgh, PA). At the end of the hypoxia incubation period, neurons were either harvested immediately or returned to normoxia for 3 h. Harvested cells were processed for RNA extraction, cDNA synthesis, and qPCR.

RESULTS

Hypoxia disturbs sterol biosynthesis

We subjected 3T3L1 cells to hypoxia in the presence or absence of ^{14}C-acetate to identify accumulated sterols in de novo and steady states, respectively. TLC of lipid extracts from ^{14}C-acetate-exposed cells revealed in hypoxia a near equal distribution of the radioactive label between cholesterol and a major lipid species that migrated similar to the lanosterol and DHL markers (**Fig. 2A, B**). GC/MS fractionation and identification of lipids in normoxia- and hypoxia-treated 3T3L1 cells in the absence of ^{14}C-acetate confirmed the presence in hypoxia of elevated DHL and lanosterol levels, which accounted for 3.1- and 2.4-fold, respectively, over cells maintained in normoxia (Fig. 2C; $P < 0.01$ each). In parallel, CYP51 and DHCR24 mRNAs were decreased by 75 and 55%, respectively, in hypoxia versus normoxia (Fig. 2D; $P < 0.01$ each). These experiments demonstrate that in hypoxic 3T3L1 cells, cholesterol biosynthesis is significantly attenuated and is coupled with a buildup of DHL and lanosterol and decreased expression of CYP51 mRNA. Furthermore, the 2.8-fold accumulation of DHL over lanosterol demonstrates that 3T3L1 cells synthesize cholesterol mainly via the Kandutsch-Russell rather than the Bloch pathway.

Hypoxia activates FoxO4 expression and nuclear translocation

Based on our previous studies involving FoxO4 in the buildup of DHL (3), we sought to determine whether FoxO4 is mobilized during hypoxia. Hypoxia treatment of 3T3L1 cells, which express HIF1a and HIF2a (**Fig. 3A**), revealed a 3.7-fold increase of FoxO4 mRNA (Fig. 3B; $P < 0.01$) and a cellular translocation of FoxO4 from the cytoplasm to the nucleus (Fig. 3C). Consistently in cellular extracts, FoxO4 was localized during hypoxia mainly in the nucleus as opposed to a uniform distribution between nucleus and cytoplasm in normoxia (Fig. 3D). This experiment demonstrates that increased transcription of the FoxO4 gene and nuclear activity of FoxO4 occur in hypoxia-treated 3T3L1 cells.

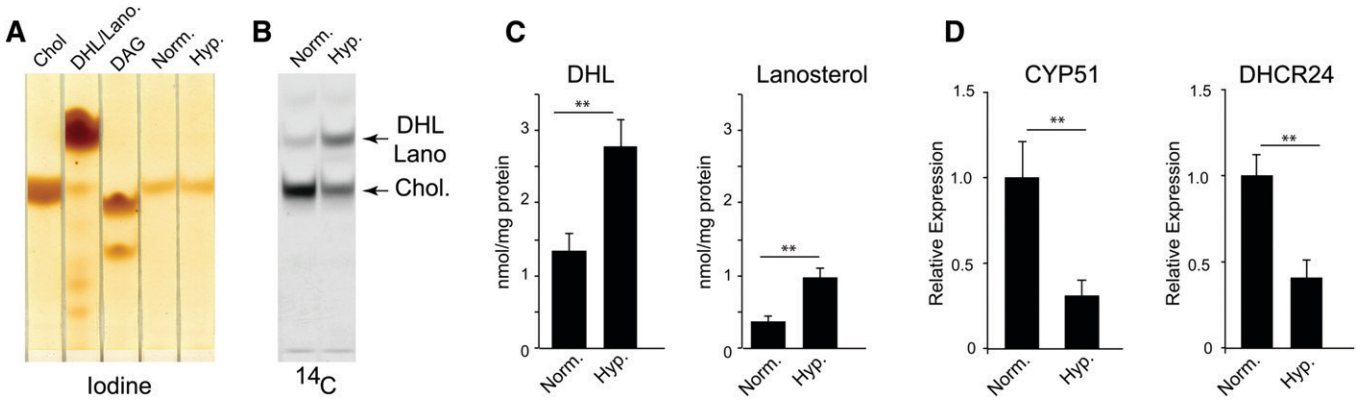

Fig. 2. Effects of hypoxia on de novo steady state sterol synthesis and mRNA expression of CYP51 and DHCR24. A: TLC fractionation of lipid extracts from cells exposed to normoxia (Norm.) or hypoxia (Hyp.) in the presence of ^{14}C-acetate. The TLC plate stained with iodine vapor (A) shows the sterol markers dihydrolanosterol (DHL), lanosterol (Lan), diacylglycerol (DAG) and cholesterol (Chol) as the major sterol in 3T3L1 cells. B: ^{14}C-labeled de novo sterol synthesis in normoxia and hypoxia shows decreased cholesterol synthesis in hypoxia-treated cells and accumulation of a lipid that comigrates with DHL. C: GC/MS reveals the identities and levels of DHL and lanosterol from cells exposed to normoxia and hypoxia. $^{**}P < 0.01$. D: Decreased mRNA expression of CYP51 and DHCR24 during hypoxia. $^{**}P < 0.01$.

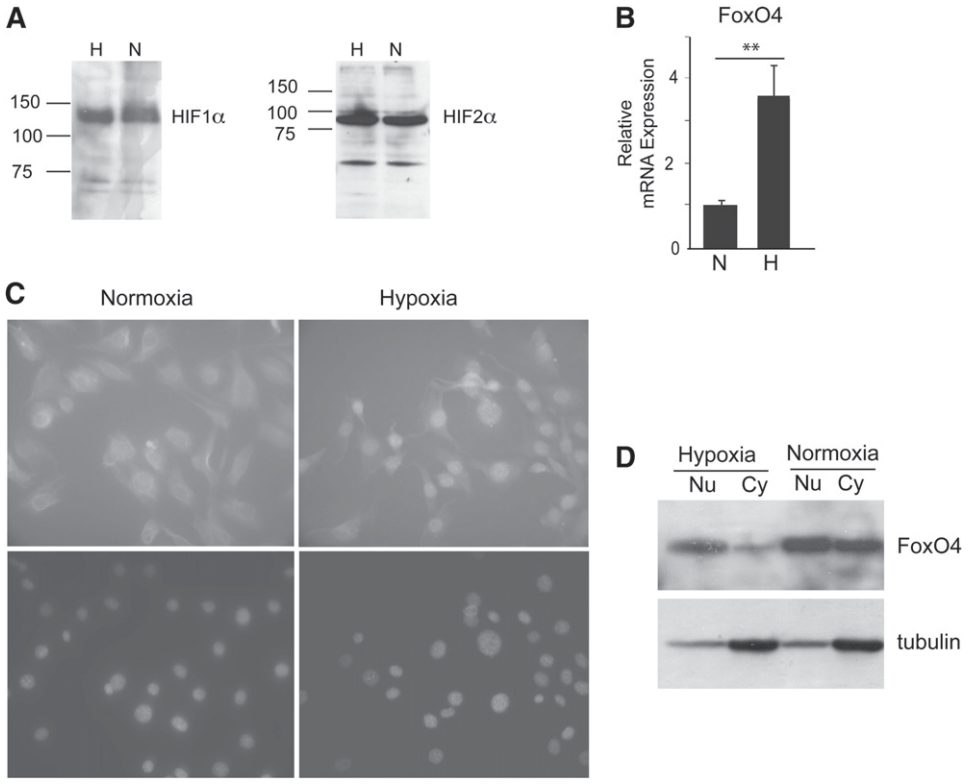

Fig. 3. Activation of FoxO4 during hypoxia. A: Western blots of confluent 3T3L1 cells probed with anti-mouse HIF1α (left panel) or HIF2α (right panel). Lower bands in both blots likely represent degradation or nonspecific proteins. B: FoxO4 mRNA levels in 3T3L1 cells during normoxia (N) and hypoxia (H). $^{**}P < 0.01$. C: Fluorescence microscopy of immunoreactive FoxO4 in 3T3L1 cells overexpressing HA-FoxO4 exposed to normoxia or hypoxia. The immunofluorescence shows the nuclear accumulation of FoxO4 under hypoxic conditions as opposed to its diffuse cytoplasmic distribution in normoxia (magnifications: normoxia 1,000×, hypoxia 400×). DAPI fluorescence is shown as control for nuclei staining. D: Localization of HA-FoxO4 in cytoplasmic (Cy) and nuclear (Nu) fractions of 3T3L1 cells overexpressing HA-FoxO4 and treated with normoxia or hypoxia. The two identical Western blots were probed with either anti-FoxO4 or anti-tubulin as a cytoplasmic control.

The mouse and human CYP51 promoters span SRE, HRE, and DBE sites

Retrieval of the human and mouse CYP51 proximal promoter regions from genome databases confirmed the presence of a sterol regulatory element (SRE) 5′-ATCACCTTCAG-3′ (9–11). This motif, which was previously shown to bind to SREBP1a in EMSAs (10), closely resembles a consensus SRE motif found among genes encoding cholesterol biosynthesis (12). However, this SRE partially differs from consensus SREs identified in a mouse genome-wide ChIP-seq study in the liver (13). In addition, we identified putative DNA binding motifs for the FoxO DBE and the HRE in both human and mouse promoters, which match their 5′-TRTTTAY-3′ and 5′-RCGTG-3′ consensus motifs, respectively (**Fig. 4**). In the mouse CYP51 promoter, the HRE and SRE sites are distant by 4 bp, whereas in the human promoter, two putative HRE sites are interspaced from the SRE by 32 bp and 108 bp. The DBE sites in the mouse and human promoters are both upstream of the SRE, occurring at 297 bp and 330 bp, respectively.

Stimulation and repression of CYP51 promoter activity by HIF2α, nSREBP2, and FoxO4

To gain insights into the potential effects of the hypoxia inducible factors HIF1α and HIF2α on the CYP51 promoter, we conducted reporter gene experiments in HEK293 cells through the transient transfection of HIF1α, HIF2α, and FoxO4 (**Fig. 5A, B**). While mRNA levels of the transfected genes nSREBP2, FoxO4, and HIF2α reached 15-fold, 1,500-fold, and 4,000-fold over endogenous levels (data not shown), HIF1α and FoxO4 had insignificant effects over the basal CYP51 promoter. However, HIF2α stimulated luciferase activity 3.8-fold over basal levels ($P < 0.01$). Moreover, in the presence of FoxO4, the stimulatory activity of HIF2α repressed luciferase activity by 55% ($P < 0.01$ each) showing that FoxO4 is a corepressor of HIF2α at the CYP51 promoter.

Examination of the CYP51 promoter with transfected nSREBP2 allowed us to evaluate these interactions under stimulated conditions (Fig. 5C). As anticipated, nSREBP2 potently stimulated activity of the CYP51 promoter, which was reflected by an increase in luciferase activity up to 10-fold over basal levels ($P < 0.01$). Interestingly in the presence of FoxO4, this activity was extended to 20-fold ($P < 0.01$), suggesting that FoxO4 and nSREBP2 cooperate together to enhance CYP51 expression. Consistent with the basal promoter transfections, HIF1α failed to show any significant activity above that of nSREBP2, whereas HIF2α alone strongly stimulated luciferase activity up to 32-fold compared with basal levels and 2.6-fold above that induced by nSREBP2 ($P < 0.01$ each). Coupled to FoxO4, the CYP51 promoter-linked

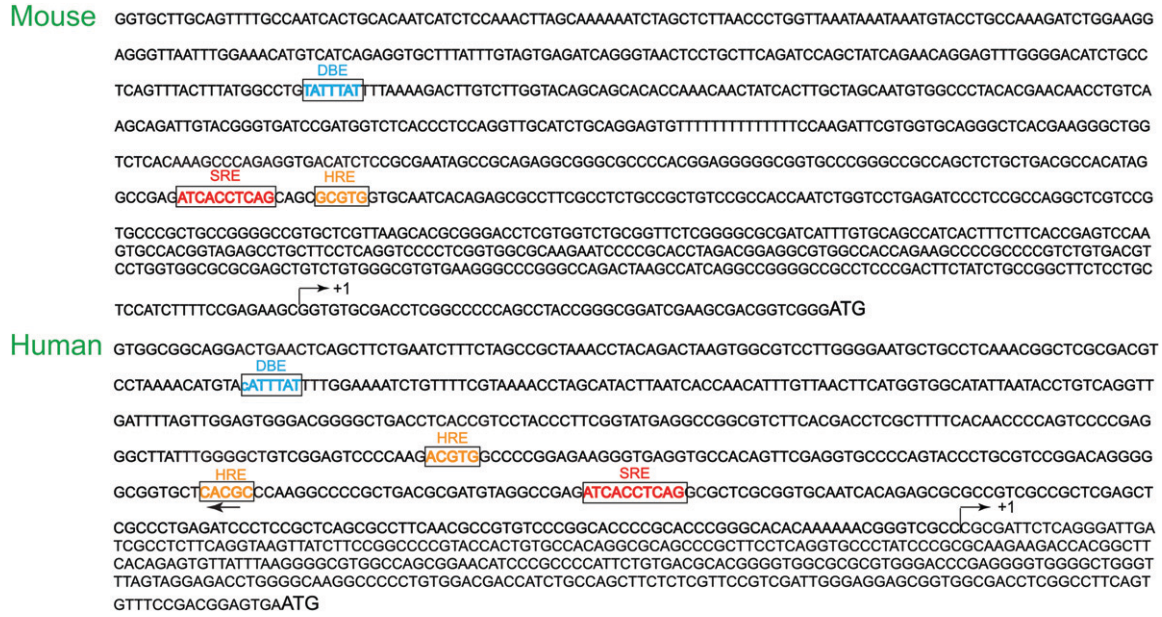

Fig. 4. DNA sequence of the mouse and human CYP51 promoters showing the DNA binding motifs (boxed) for the SRE, HRE, and DBE. All motifs match their consensus sequences except for the human DBE site, which deviates by a single nucleotide at its 5′ end. The arrows on the DNA sequences point to the initiation of transcription that precedes the initiation codon ATG.

luciferase activities resulting from HIF2α transfection were repressed almost down to the levels of nSREBP2 ($P < 0.01$), reinforcing the possibility that FoxO4 acts as a corepressor of HIF2α activity. Whereas transient overexpression of the proteins carried by the plasmids is not likely to faithfully reproduce endogenous levels of stimulation and suppression of promoter activity, they nonetheless indicate protein interactions, and in this context suggest that FoxO4 is a coactivator of nSREBP2 and a corepressor of HIF2α.

nSREBP2, HIF2α, and FoxO4 bind to the CYP51 promoter in 3T3L1 cells

To determine whether FoxO4 and HIF2α occupy the promoter region that encompasses their respective DNA motifs, we carried out ChIP assays from chromatin preparations of 3T3L1 cells stably expressing HA-FoxO4 (3). These cells express HIF2α in normoxia and hypoxia (**Fig. 6A**) and are thus appropriate for ChIP with anti-HIF2α under normoxic conditions. Thus, following ChIP with anti-HA, anti-FoxO4, or anti-HIF2α (Fig. 6B–D) the bound DNA was released and amplified with primers bracketing the DBE or HRE sequences. Figure 6C shows amplification of the 150 bp PCR product bracketing the DBE motif from chromatin immunoprecipitated with anti-HA or anti-FoxO4, but not with chromatin immunoprecipitated with a nonspecific IgG antibody serving as a negative control. Similarly, PCR amplification of the HRE region with chromatin immunoprecipitated with anti-HIF2α resulted in

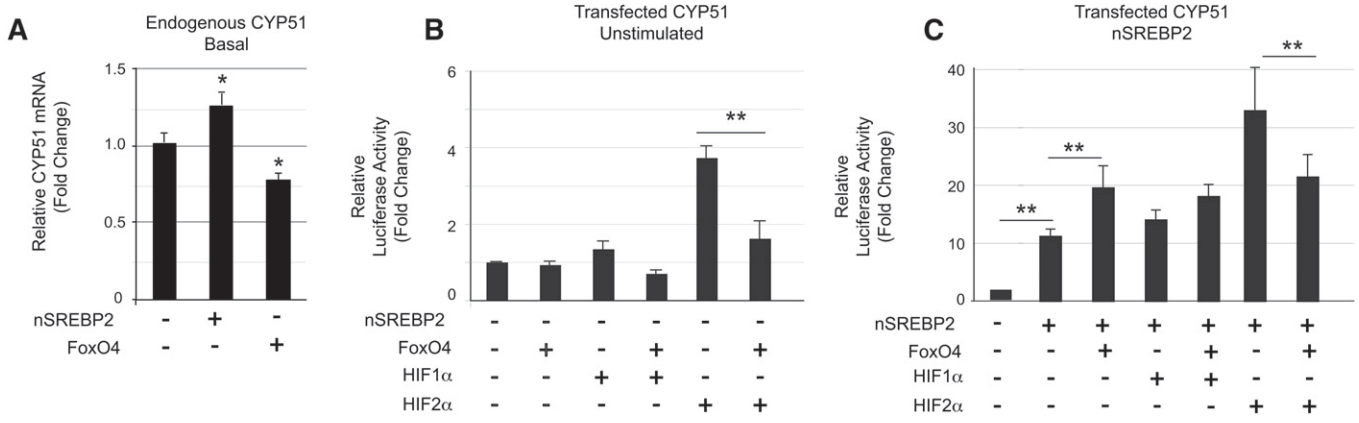

Fig. 5. Effects of transfected nSREBP2 and FoxO4 in HEK293 cells on the endogenous human CYP51 promoter (A) and with HIF1α and HIF2α on the cotransfected mouse CYP51 promoter. *$P < 0.05$. (B, C) linked to the luciferase reporter gene in basal (B) and nSREBP2 stimulated (C) HEK293 cells. A: Shows changes in endogenous CYP51 mRNA levels. B, C: Shows ratios of Firefly to Renilla luciferase activities that are normalized to cells transfected with only the CYP51 promoter reporter gene. Data represent the pooled means and SEMs of five to seven independent experiments, each performed in triplicate. The presence or absence of the indicated plasmids in each transfection is denoted with (+) and (−), respectively. **$P < 0.01$.

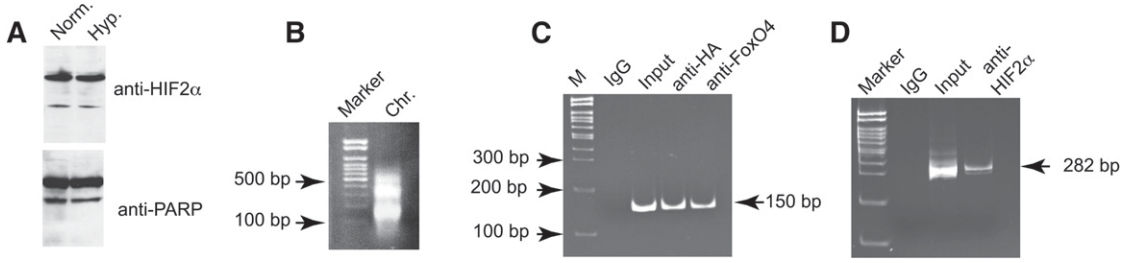

Fig. 6. ChIP assays of 3T3L1 HA-FoxO4 expressing HIF2α. A: Western blot of nuclear extracts from 3T3L1 cells exposed to normoxia (Norm.) and hypoxia (Hyp.) and probed with anti-HIF2α. A parallel blot was also prepared and reacted with anti-PARP as a control for nuclear protein expression. The lower intensity bands in both blots are likely degradation products of HIF2α and PARP. B: Gel electrophoresis of the chromatin (Chr.) preparation from HA-FoxO4 3T3L1 cells is shown next to a 100 bp ladder DNA marker (Marker). C, D: Gel electrophoresis of PCR products from chromatin immunoprecipitated with anti-HA, anti-FoxO4, and anti-HIF2α. Nonimmunoprecipitated chromatin (5% input) is shown as positive control and an isotype-specific IgG as negative control. The sizes of the resulting PCR products are shown next to each gel relative to the DNA marker (M).

the 282 bp amplification product (Fig. 6D). These results demonstrate that FoxO4 and HIF2α bind each to the DNA regions that span their respective putative DBE and HRE recognition elements in the CYP51 promoter of 3T3L1 cells.

Physical interaction of FoxO4 with nSREBP2 and HIF2α

We performed EMSAs to assess whether the SRE, HRE, and DBE motifs represent authentic DNA binding sites for their respective transcription factors and to determine whether they interact together in supershift assays. ^{32}P-labeled double-stranded oligonucleotide probes spanning the SRE, HRE, or DBE sites were used in the gel shift assays with FoxO4, nSREBP2 (**Fig. 7A**), and HIF2α (Fig. 7B). Figure 7C shows that nSREBP2, but not FoxO4, shifted the SRE probe. However, FoxO4 supershifted the SRE probe/nSREBP2 complex, indicating that it binds to nSREBP2. Binding specificity of nSREBP2 to its SRE motif was demonstrated by competition assays, which show the increasingly reduced SRE probe shift in the presence of increasing amounts of unlabeled SRE probe. Conversely, unlabeled mutant SRE probes slightly competed with the binding of nSREBP2 to its radiolabeled wild-type probe. Overall, these assays demonstrate that nSREBP2 binds specifically to the SRE motif and that FoxO4 binds to nSREBP2.

Figure 7D shows that FoxO4, but not nSREBP2, shifted the wild-type DBE probe. However, nSREBP2 supershifted the DBE probe/FoxO4 complex, indicating that nSREBP2 interacts with FoxO4, a finding consistent with the reciprocal binding shown below in **Fig. 8**. Binding specificity of FoxO4 to DBE was demonstrated by the lack of FoxO4 binding to a probe with a mutated DBE.

To interrogate the HRE site, we used a probe that only spans the HRE motif and in vitro translated HA-HIF2α. The presence of the HIF heterodimer partner aryl hydrocarbon receptor nuclear translocator (ARNT) was detected in the TNT lysate (Fig. 7B), as also shown by others (14). Figure 7E shows that HA-HIF2α shifted the HRE probe. Binding specificity of HIF2α to the HRE probe was confirmed with unlabeled wild-type and mutant probe competition assays. Thus, a gradual loss of HIF2α binding to the ^{32}P-labeled HRE probe was competed out in the presence of increasing amounts of wild-type HRE unlabeled probe. Conversely, binding of the HA-HIF2α to the radiolabeled HRE probe was unaffected by the mutant unlabeled HRE probe. Antibody supershift assays with anti-HA (tagged onto HIF2α), anti-HIF2α, and anti-ARNT confirmed the specificities of the protein interactions with the HRE probe. Altogether, these findings demonstrate that the HIF2α/ARNT complex binds to the HRE.

To determine whether nSREBP2, HIF2α, and FoxO4 cooperate altogether at the SRE site, we assessed their interactions with the SRE probe (Fig. 7F). Consistent with the above findings, nSREBP2 shifted the SRE probe but not FoxO4 or HIF2α. However, each of FoxO4 and HIF2α supershifted separately the nSREBP2/SRE probe complex, indicating distinct interactions with nSREBP2. Most notably, the simultaneous presence of FoxO4 and HIF2α with the nSREBP2/SRE probe complex resulted in a ternary complex that could barely migrate into the gel due to its large size. This experiment demonstrates that nSREBP2, FoxO4, and HIF2α interact altogether at the SRE site to form a ternary complex.

To further establish the interaction of nSREBP2 and FoxO4, we performed cotransfections of nSREBP2 and FoxO4 in HEK293 cells followed with pull-down and coimmunoprecipitation assays. nSREBP2 was tagged with 6xHis for pull-down assays and with the V5 tag for antibody detection. For FoxO4, we used three different constructs, human HA-FoxO4, mouse FoxO4-3xHA, and human FLAG-FoxO4. Expression of the intended proteins following transfection was confirmed by Western blotting from whole cell lysates with anti-FoxO4 and anti-V5 (Fig. 8A, B). Pull-down assays of nSREBP2 cotransfected with FoxO4-HA, followed by immunodetection of the pulled-down products with anti-FoxO4 revealed the pull-down of FoxO4 only in cotransfections with nSREBP2 (Fig. 8A, lane 4). Conversely, immunoprecipitation of FoxO4 revealed the detection of nSREBP2-V5 (with anti-V5) only in cotransfections (Fig. 8B, lanes 5, 6) with human and mouse FoxO4. This experiment additionally confirms the interactions of nSREBP2 and FoxO4 and extends this interaction to both mouse and human FoxO4.

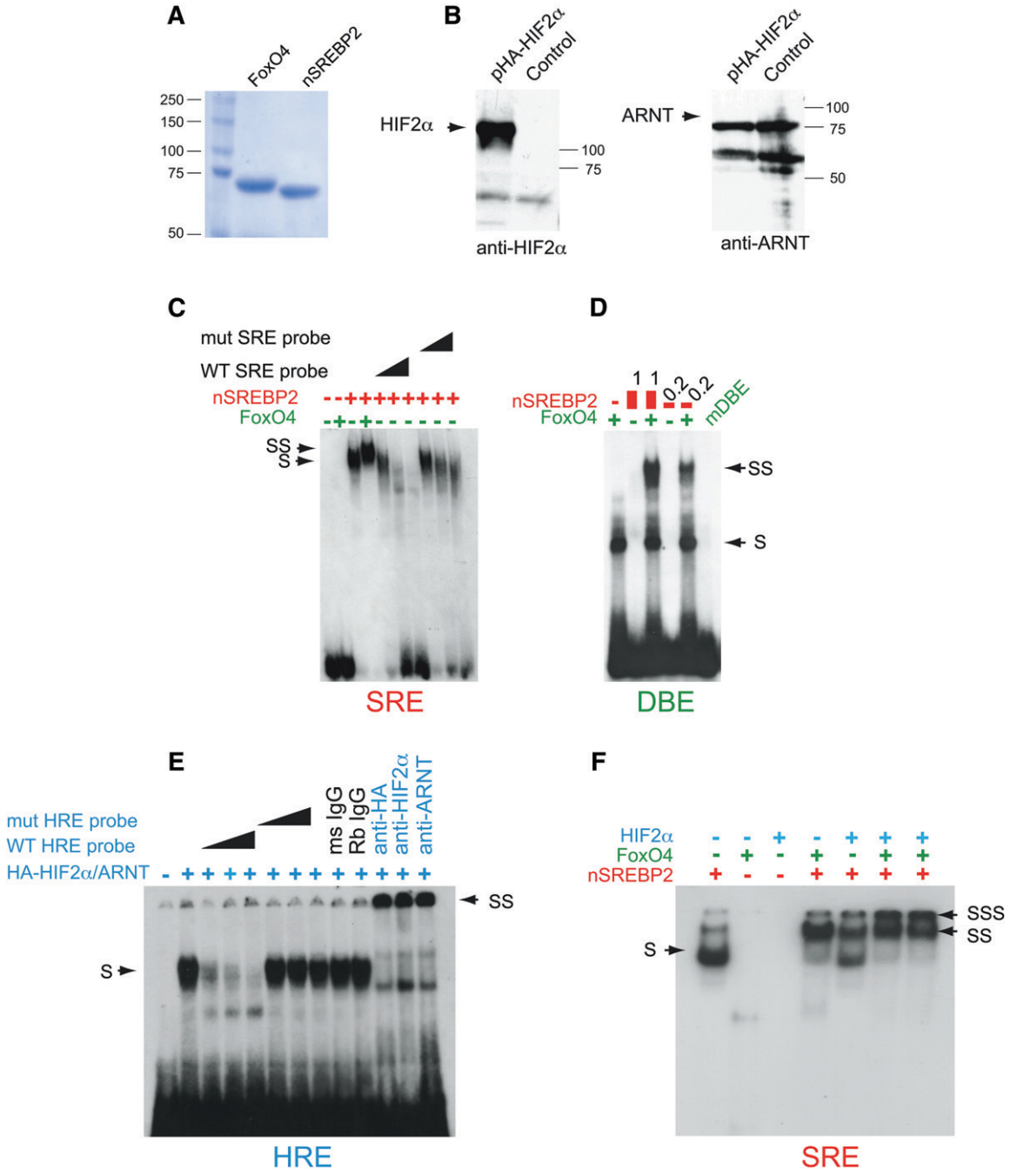

Fig. 7. EMSAs of SRE, DBE, and HRE double-stranded probes with nSREBP2, FoxO4, and HIF2α. In all assays, the presence or absence of each protein in the incubation mix is indicated with (+) or (−), respectively. Probe shifts, supershifts, and super supershifts are indicated by S, SS, and SSS, respectively. A: Polyacrylamide gel stained with Coomassie blue showing the purity of the recombinant proteins FoxO4 and nSREBP2 used in the gel shift assays. B: Western blots with anti-HIF2α and anti-ARNT of the TNT reaction with added pHA-HIF2α expression plasmid or without (control), demonstrating synthesis of HA-HIF2α and presence of ARNT in the TNT lysate. The lower bands in both lanes of the HIF2α blot are nonspecific and originate from the TNT extract. The band around 60 kDa in the ARNT blot is likely to be a degradation product of ARNT. C: Shift assays of the SRE probe with FoxO4, nSREBP2, or both. Note the supershift (SS) of nSREBP2 and FoxO4. Competition assays with increasing amounts of unlabeled excess wild-type SRE (WT SRE) or mutant SRE (mut SRE) probes are indicated with the filled triangles, showing competitive binding to the WT but not the mutant probe. D: Shift assays of the DBE probe with FoxO4, nSREBP2, or both. The relative amounts of nSREBP2 are indicated by 1 and 0.2. nSREBP2 supershifts the FoxO4 bound probe at 1× and 0.2× the amount of input protein. Note the absence of probe binding to the mutant DBE probe (mDBE). E: Shift assays of the HRE probe with HA-HIF2α. Competition assays with increasing amounts of unlabeled excess wild-type HRE (WT HRE) or mutant HRE (mut HRE) probes are indicated with the filled triangles, showing specificity to the WT but not the mutant probe. Antibody supershift assays also denoting specificity of the DNA-protein complex are shown with anti-HA (the tag on HA-HIF2α), anti-HIF2α, or anti-ARNT (the HIF2α heterodimer partner). Mouse and rabbit specific isotype antibodies serve as negative antibody controls and are denoted by ms IgG and Rb IgG, respectively. F: Interactions of FoxO4 and HIF2α with the SRE probe/nSREBP2 complex (denoted with S). HIF2α supershifts the SRE probe/nSREBP2 complex (SS) while the addition of FoxO4 further shifts the SRE probe/nSREBP2/HIF2α complex (SSS). The resulting large ternary complex migrates minimally into the polyacrylamide gel.

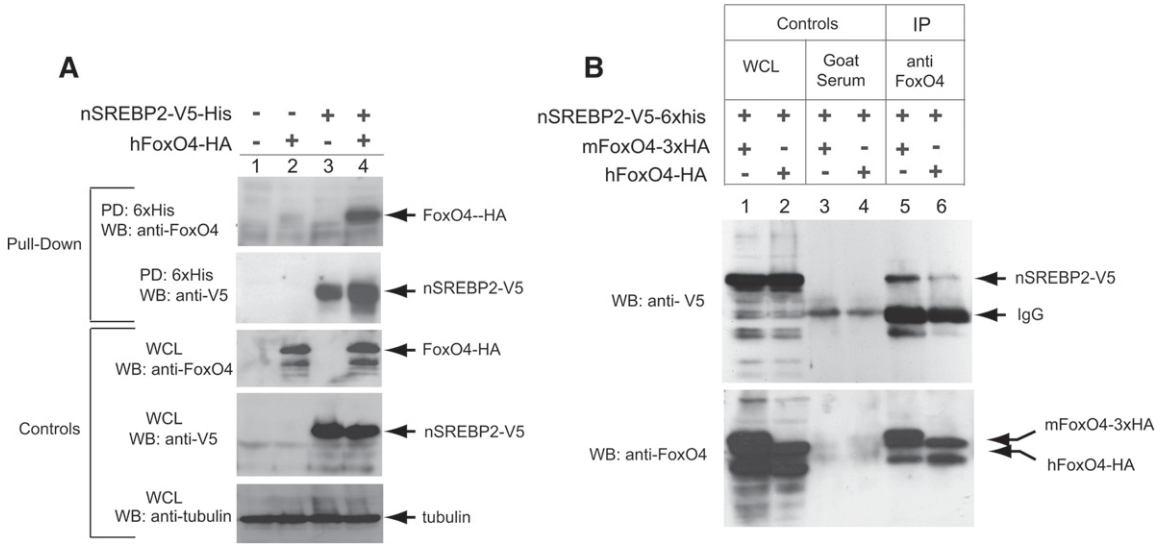

Fig. 8. Pull-down (PD) of nSREBP2 with FoxO4 and coIP of FoxO4 with nSREBP2. A: Lane 1 is a no transfection control, lanes 2 and 3 are from single transfections of FoxO4-HA and nSREBP2-V5-His, respectively. Lane 4 is from a cotransfection of FoxO4-HA and nSREBP2-V5-His. Two Western blots (WB) of whole cell lysate (WCL) controls not pulled down demonstrate successful transfections of FoxO4-HA and nSREBP2-V5-His, whereas the tubulin Western blot shows equal protein loading. Detection of FoxO4 in lane 4 of the lysate pulled-down with the Ni-NTA beads and thus nSREBP2-V5-6xHis demonstrates coIP of FoxO4 and nSREBP2-V5-6xHis. B: Immunoprecipitation (IP) of mouse FoxO4 (mFoxO4-3xHA) and human FoxO4 (hFoxO4-HA) followed by Western blotting with anti-V5 tagging nSREBP2. Lanes 1 and 2 are from transfected lysates that are not immunoprecipitated. The blots show the presence of all three transfected proteins. Note that the mouse FoxO4-3xHA protein migrates slightly slower than human FoxO4-HA, thus adding specificity to the coIP. Lanes 3 and 4 are from lysates immunoprecipitated with a nonspecific goat serum, showing background IgG with anti-V5 and no reactivity with anti-FoxO4. Lanes 5 and 6 are from lysates immunoprecipitated with anti-FoxO4 and detected with anti-V5 as a tag for nSREBP2, showing the coIP of nSREBP2 with mouse (lane 5) and human FoxO4 (lane 6). Lanes 5 and 6 of the Western blot probed with anti-FoxO4 serve as positive controls for the immunoprecipitation with anti-FoxO4.

Roles of FoxO4 in the stimulation and repression of CYP51 in ob/ob mice and cortical neurons of fetal mice

The relative expressions of the hypoxia-sensitive genes VEGF, HIF1α, and HIF2α (**Fig. 9A**) were not significantly different between lean and ob/ob mice at 8 weeks of age despite a body weight difference of 26.4 g, representing a large buildup of adipose tissue mass in ob/ob mice. Thus, at least at this age and with the assays used in this experiment, the adipose tissue did not appear to be in a hypoxic state. However, FoxO4 mRNA levels were 50% lower in ob/ob versus lean mice concomitant with a 3.5-fold increase in CYP51 expression levels. Similarly, SREBP2 and HMG-CoA synthase (HMGCS) were increased in ob/ob mice by 5.2-fold and 1.9-fold, respectively, over lean mice (Fig. 9B). Overall, these results show that in the visceral WAT of ob/ob mice at 8 weeks of age, low FoxO4 expression is associated with an increase in CYP51 expression, thus vindicating the in vivo inverse relationship between FoxO4 and CYP51 expressions.

The response of primary cortical neurons exposed to hypoxia was evident by the increase in VEGF, HIF1α, HIF2α, and FoxO4 mRNA, which consisted of 7.1-, 2.1-, 4.4-, and 15.2-fold, respectively, in hypoxia versus normoxia (Fig. 9C). Exposure of cortical neurons to normoxia following hypoxia reversed to a large extent the hypoxia-induced response demonstrating specificity. Similarly, expressions of the cholesterol biosynthesis genes SREBP2, HMGCS, and HMGCR were stimulated in hypoxia by 2.5-, 2.8-, and 2.4-fold, respectively, over normoxia and reversed to basal or lower levels by reoxygenation. On the other hand, CYP51 mRNA levels were minimally stimulated with hypoxia by only 1.4-fold, further substantiating the repressive effects of elevated FoxO4, HIF2α, and SREBP2 on CYP51 expression (Fig. 9D).

DISCUSSION

Cholesterol biosynthesis is an oxygen-demanding two-arm pathway. In the proximal mevalonate pathway, a single O_2 molecule is required for the conversion of squalene to lanosterol. However, in the distal pathway or so-called late steps, 10 additional O_2 molecules are consumed to complete the synthesis of a cholesterol molecule (15). Thus, reduced oxygen availability, as in hypoxic states, is likely to be coupled with regulatory mechanisms that conserve O_2 to ensure cell survival (16). The demethylation of lanosterol at C14 by CYP51 requires three molecules of O_2 and constitutes the first and second steps in the Bloch and Kandutsch-Russell arms of the distal pathway, respectively. While the HMG-CoA reductase step is the rate-limiting step of the proximal pathway, demethylation at C14 of lanosterol may represent a similar rate-limiting step in the distal pathway. The link between these two rate-limiting steps is exemplified by the hypoxia-mediated build-up of lanosterol and DHL that act as negative feedback drivers to mediate the degradation

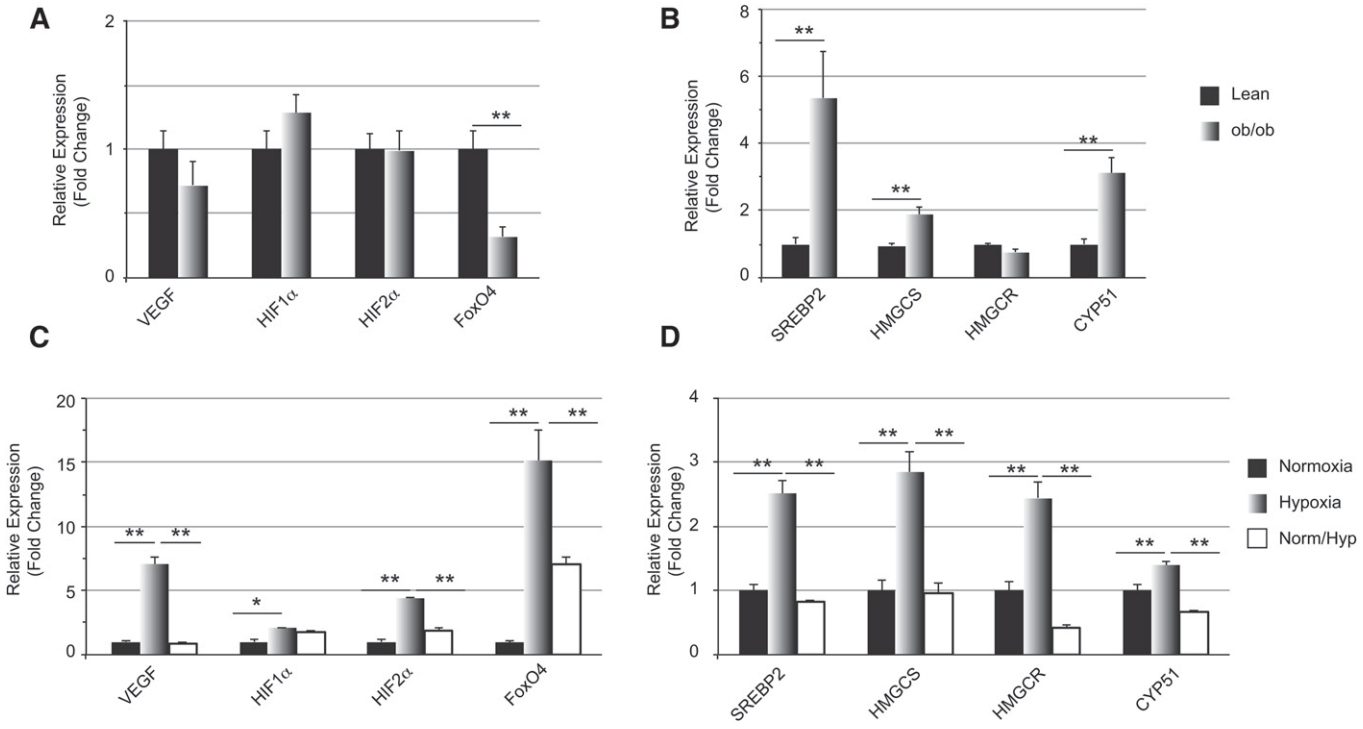

Fig. 9. mRNA levels of VEGF, HIF1α, HIF2α, and FoxO4, and cholesterol biosynthesis genes (nSREBP2, HMGCS, HMGCR and CYP51) from visceral adipose tissue of C57BL lean and C57BL ob/ob mice (A) and from mouse primary cortical neurons exposed to normoxia, hypoxia for 3 h or hypoxia for 3 h followed by normoxia for 3 h (B). $*P < 0.05$; $**P < 0.01$.

of HMG-CoA reductase and repress cholesterol biosynthesis (2, 17, 18).

Hypoxia is a characteristic stress feature of a number of pathophysiological conditions such as cancer, stroke, and cardiac ischemia (19). The cellular response to hypoxic stress consists of multiple defense mechanisms that cells invoke to alleviate the damaging effects of the environment and cope with survival. This effect is largely mediated by the hypoxia inducible transcription factors HIF1α and HIF2α, which bind to an identical DNA core motif (5′-RCGTG-3′) but yet regulate distinct target genes (16, 20). We have previously shown that repression of CYP51 gene expression occurs in confluent mouse 3T3L1 cells overexpressing FoxO4, resulting in the accumulation of substantial amounts of the intermediary sterol DHL (3). We hypothesized that hypoxic-like conditions of confluent cell growth might allow FoxO4 to participate in the down-regulation of CYP51. Supporting this hypothesis is our present finding that during hypoxia FoxO4 mRNA is induced and that it translocates from the cytoplasm to the nucleus, hinting to its increased transcriptional activity (21) in deprived oxygen states.

CYP51 expression is largely stimulated by nSREBP2 and our studies now show that HIF2α and the nSREBP2/FoxO4 complex also potently activate it. It is interesting to point out that the stimulatory effect of HIF2α, but not HIF1α, on the CYP51 linked luciferase activity occurs despite the fact that they both recognize the same DNA binding motif. While the nature of the disparity between HIF1α and HIF2α is currently unknown at the CYP51 promoter, this differential effect has been previously noted (22, 23) and could result from their distinct transactivation domains that provide docking sites for separate cofactors (24). In this context, the greater response of the CYP51 promoter to HIF2α versus HIF1α could lie in its interactions with nSREBP2 and FoxO4. A candidate for the regulation of this complex could be Sirt1, which deacetylates and activates independently HIF2α (25) and FoxO4 (26, 27). In this vein, roles for deacetylases in cholesterol biosynthesis were demonstrated for the transcription factor YY1, which recruits histone deacetylase 3 to repress lanosterol synthase transcription (28), and for Sirt6, which is recruited by FoxO3 to the SREBP2 promoter (29).

The roles of HIF2α and FoxO4 in activating CYP51 expression encompass those of other positive regulators of CYP51, such as the cyclic AMP responsive modulators ((9,10,30)) and the heme binding protein PGRMC1 (31). On the other hand, repression of CYP51 expression occurs, as shown by this study, with the HIF2α/FoxO4 and nSREBP2/FoxO4/HIF2α complexes, resulting in the accumulation of lanosterol and DHL (3) and to the ubiquitin-mediated degradation of HMG-CoA reductase (2, 17, 18), leading altogether to decreased cholesterol biosynthesis.

Even though the proposed interactions of FoxO4 with HIF2α and nSREBP2 are largely based on in vitro studies, the inverse relationship between FoxO4 and CYP51 expressions in the adipose tissue of ob/ob mice and hypoxia-exposed fetal mouse cortical neurons adds credence to this model by extending its role to in vivo, potentially to brain ischemia.

A model for stimulation and repression of CYP51 gene expression is proposed in **Fig. 10** and takes into account

the various complexes identified in this study and the nearby chromatin configuration that juxtaposes DNA-bound FoxO4 close to nSREBP2 and HIF2α. In this scheme, stimulation of CYP51 expression occurs when nSREBP2, HIF2α, or both bind to their respective SRE and HRE motifs. Additional stimulation could occur with the recruitment of FoxO4 by nSREBP2, either directly or following binding to its DBE site. Repression of CYP51 would occur with the direct interaction of FoxO4 with HIF2α or via the binding of FoxO4 to its DBE site. Similarly, formation of the trimeric complex FoxO4-nSREBP2-HIF2α would further contribute to CYP51 repression.

The ability of the FoxO transcription factors to cooperate as accessory proteins to other transcription factors widens their biological roles and thus many FoxO binding partners have been identified [for a review see (32)]. Interestingly, interaction of FoxO4 with the transcription factors myocardin and serum response factor also results in a ternary complex that represses smooth muscle cell gene expression (33). Moreover, FoxO1, FoxO3a, and FoxO4 act as coactivators when they partner with Smad3 and Smad4 in a TGFβ-dependent pathway to turn on the growth inhibitory gene p21Cip1 (34). Furthermore, FoxOs associate with multiple steroid nuclear hormone receptors to repress or activate target gene expression (35–38).

Altogether, our studies extend the stimulatory and repressive roles of FoxO4 and potentially other FoxO factors, as accessory proteins in transcriptional complexes that regulate CYP51 expression and subsequent activity levels. Because nSREBP2 stimulates the expression of multiple cholesterol biosynthesis genes, it is conceivable that the interaction of FoxO4 with nSREBP2 could also encompass additional genes in this pathway, and it remains to be determined whether HIF1α or HIF2α participate in this process. In addition, the FoxO transcription factors FoxO1 and FoxO3a, which share homologies to FoxO4, may also broaden the roles of FoxOs in cholesterol biosynthesis. Elucidation of the FoxO4 protein domains that interact with nSREBP2 and HIF2α remain to be determined, but when elucidated might uncover the specificities and/or redundancies of FoxOs in regulating cholesterol biosynthesis.

Lastly, the extension of our findings from the mouse to the human CYP51 promoter is likely to be similar owing to the presence of DNA binding motifs for SRE, HRE, and DBE in the human CYP51 promoter region. In aggregate, our studies demonstrate that FoxO4 participates with nSREBP2 and HIF2α in the regulation of CYP51 during hypoxic states.

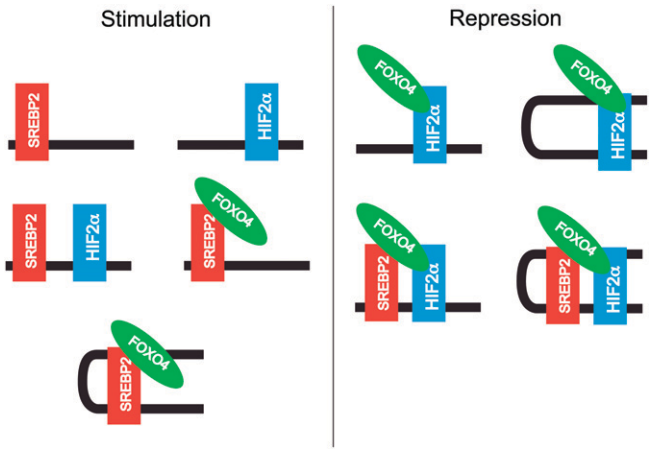

Fig. 10. Model for the stimulation and repression of CYP51 with nSREBP2, HIF2α, FoxO4, and their cooperative complexes. The three transcription factors are depicted binding to their respective DNA binding sites. The relatively distant binding of FoxO4 to its DBE is denoted by the looping-out of DNA bringing FoxO4 close to its cofactors. Stimulation of CYP51 expression occurs with nSREBP2, HIF2α, or both and with the FoxO4/nSREBP2 complex. Repression of CYP51 expression occurs with the ternary complex nSREBP2/FoxO4/HIF2α or with HIF2α/FoxO4.

The authors thank Drs. Ruth Welti, Libin Yao, and Thilani Samarakoon for GC/MS lipid analysis and are grateful to Dr. Kenneth Feingold for critical reading, suggestions, and comments on the manuscript.

REFERENCES

1. Strömstedt, M., D. Rozman, and M. R. Waterman. 1996. The ubiquitously expressed human CYP51 encodes lanosterol 14 alpha-demethylase, a cytochrome P450 whose expression is regulated by oxysterols. *Arch. Biochem. Biophys.* **329:** 73–81.
2. Song, B. L., N. B. Javitt, and R. A. DeBose-Boyd. 2005. Insig-mediated degradation of HMG CoA reductase stimulated by lanosterol, an intermediate in the synthesis of cholesterol. *Cell Metab.* **1:** 179–189.
3. Zhu, J., K. Mounzih, E. F. Chehab, N. Mitro, E. Saez, and F. F. Chehab. 2010. Effects of FoxO4 overexpression on cholesterol biosynthesis, triacylglycerol accumulation, and glucose uptake. *J. Lipid Res.* **51:** 1312–1324.
4. Bligh, E. G., and W. J. Dyer. 1959. A rapid method of total lipid extraction and purification. *Can. J. Biochem. Physiol.* **37:** 911–917.
5. Kondo, K., J. Klco, E. Nakamura, M. Lechpammer, and W. G. Kaelin, Jr. 2002. Inhibition of HIF is necessary for tumor suppression by the von Hippel-Lindau protein. *Cancer Cell.* **1:** 237–246.
6. Yan, Q., S. Bartz, M. Mao, L. Li, and W. G. Kaelin, Jr. 2007. The hypoxia-inducible factor 2alpha N-terminal and C-terminal transactivation domains cooperate to promote renal tumorigenesis in vivo. *Mol. Cell. Biol.* **27:** 2092–2102.
7. Chehab, F. F., M. E. Lim, and R. Lu. 1996. Correction of the sterility defect in homozygous obese female mice by treatment with the human recombinant leptin. *Nat. Genet.* **12:** 318–320.
8. Jiang, X., D. Mu, C. Manabat, A. A. Koshy, S. Christen, M. G. Tauber, Z. S. Vexler, and D. M. Ferriero. 2004. Differential vulnerability of immature murine neurons to oxygen-glucose deprivation. *Exp. Neurol.* **190:** 224–232.
9. Halder, S. K., M. Fink, M. R. Waterman, and D. Rozman. 2002. A cAMP-responsive element binding site is essential for sterol regulation of the human lanosterol 14alpha-demethylase gene (CYP51). *Mol. Endocrinol.* **16:** 1853–1863.
10. Rozman, D., M. Fink, G. M. Fimia, P. Sassone-Corsi, and M. R. Waterman. 1999. Cyclic adenosine 3′,5′-monophosphate(cAMP)/cAMP-responsive element modulator (CREM)-dependent regulation of cholesterogenic lanosterol 14alpha-demethylase (CYP51) in spermatids. *Mol. Endocrinol.* **13:** 1951–1962.
11. Debeljak, N., S. Horvat, K. Vouk, M. Lee, and D. Rozman. 2000. Characterization of the mouse lanosterol 14alpha-demethylase (CYP51), a new member of the evolutionarily most conserved cytochrome P450 family. *Arch. Biochem. Biophys.* **379:** 37–45.
12. Sharpe, L. J., and A. J. Brown. 2013. Controlling cholesterol synthesis beyond 3-hydroxy-3-methylglutaryl-CoA reductase (HMGCR). *J. Biol. Chem.* **288:** 18707–18715.
13. Seo, Y. K., T. I. Jeon, H. K. Chong, J. Biesinger, X. Xie, and T. F. Osborne. 2011. Genome-wide localization of SREBP-2 in hepatic chromatin predicts a role in autophagy. *Cell Metab.* **13:** 367–375.

14. Isaacs, J. S., Y. J. Jung, and L. Neckers. 2004. Aryl hydrocarbon nuclear translocator (ARNT) promotes oxygen-independent stabilization of hypoxia-inducible factor-1alpha by modulating an Hsp90-dependent regulatory pathway. *J. Biol. Chem.* **279:** 16128–16135.
15. Summons, R. E., A. S. Bradley, L. L. Jahnke, and J. R. Waldbauer. 2006. Steroids, triterpenoids and molecular oxygen. *Philos. Trans. R. Soc. Lond. B Biol. Sci.* **361:** 951–968.
16. Semenza, G. L. 2009. Regulation of oxygen homeostasis by hypoxia-inducible factor 1. *Physiology (Bethesda).* **24:** 97–106.
17. Sever, N., B. L. Song, D. Yabe, J. L. Goldstein, M. S. Brown, and R. A. DeBose-Boyd. 2003. Insig-dependent ubiquitination and degradation of mammalian 3-hydroxy-3-methylglutaryl-CoA reductase stimulated by sterols and geranylgeraniol. *J. Biol. Chem.* **278:** 52479–52490.
18. Nguyen, A. D., J. G. McDonald, R. K. Bruick, and R. A. DeBose-Boyd. 2007. Hypoxia stimulates degradation of 3-hydroxy-3-methylglutaryl-coenzyme A reductase through accumulation of lanosterol and hypoxia-inducible factor-mediated induction of insigs. *J. Biol. Chem.* **282:** 27436–27446.
19. Semenza, G. L. 2000. HIF-1: mediator of physiological and pathophysiological responses to hypoxia. *J. Appl. Physiol.* **88:** 1474–1480.
20. Mole, D. R., C. Blancher, R. R. Copley, P. J. Pollard, J. M. Gleadle, J. Ragoussis, and P. J. Ratcliffe. 2009. Genome-wide association of hypoxia-inducible factor (HIF)-1alpha and HIF-2alpha DNA binding with expression profiling of hypoxia-inducible transcripts. *J. Biol. Chem.* **284:** 16767–16775.
21. Biggs 3rd, W. H., J. Meisenhelder, T. Hunter, W. K. Cavenee, and K. C. Arden. 1999. Protein kinase B/Akt-mediated phosphorylation promotes nuclear exclusion of the winged helix transcription factor FKHR1. *Proc. Natl. Acad. Sci. USA.* **96:** 7421–7426.
22. Hu, C. J., L. Y. Wang, L. A. Chodosh, B. Keith, and M. C. Simon. 2003. Differential roles of hypoxia-inducible factor 1alpha (HIF-1alpha) and HIF-2alpha in hypoxic gene regulation. *Mol. Cell. Biol.* **23:** 9361–9374.
23. Loboda, A., A. Jozkowicz, and J. Dulak. 2010. HIF-1 and HIF-2 transcription factors–similar but not identical. *Mol. Cells.* **29:** 435–442.
24. Hu, C. J., A. Sataur, L. Wang, H. Chen, and M. C. Simon. 2007. The N-terminal transactivation domain confers target gene specificity of hypoxia-inducible factors HIF-1alpha and HIF-2alpha. *Mol. Biol. Cell.* **18:** 4528–4542.
25. Dioum, E. M., R. Chen, M. S. Alexander, Q. Zhang, R. T. Hogg, R. D. Gerard, and J. A. Garcia. 2009. Regulation of hypoxia-inducible factor 2alpha signaling by the stress-responsive deacetylase sirtuin 1. *Science.* **324:** 1289–1293.
26. van der Horst, A., L. G. Tertoolen, L. M. de Vries-Smits, R. A. Frye, R. H. Medema, and B. M. Burgering. 2004. FOXO4 is acetylated upon peroxide stress and deacetylated by the longevity protein hSir2(SIRT1). *J. Biol. Chem.* **279:** 28873–28879.
27. Brunet, A., L. B. Sweeney, J. F. Sturgill, K. F. Chua, P. L. Greer, Y. Lin, H. Tran, S. E. Ross, R. Mostoslavsky, H. Y. Cohen, et al. 2004. Stress-dependent regulation of FOXO transcription factors by the SIRT1 deacetylase. *Science.* **303:** 2011–2015.
28. Villagra, A., N. Ulloa, X. Zhang, Z. Yuan, E. Sotomayor, and E. Seto. 2007. Histone deacetylase 3 down-regulates cholesterol synthesis through repression of lanosterol synthase gene expression. *J. Biol. Chem.* **282:** 35457–35470.
29. Tao, R., X. Xiong, R. A. DePinho, C. X. Deng, and X. C. Dong. 2013. Hepatic SREBP-2 and cholesterol biosynthesis are regulated by FoxO3 and Sirt6. *J. Lipid Res.* **54:** 2745–2753.
30. Kosir, R., U. P. Zmrzljak, T. Bele, J. Acimovic, M. Perse, G. Majdic, C. Prehn, J. Adamski, and D. Rozman. 2012. Circadian expression of steroidogenic cytochromes P450 in the mouse adrenal gland–involvement of cAMP-responsive element modulator in epigenetic regulation of Cyp17a1. *FEBS J.* **279:** 1584–1593.
31. Hughes, A. L., D. W. Powell, M. Bard, J. Eckstein, R. Barbuch, A. J. Link, and P. J. Espenshade. 2007. Dap1/PGRMC1 binds and regulates cytochrome P450 enzymes. *Cell Metab.* **5:** 143–149.
32. van der Vos, K. E., and P. J. Coffer. 2008. FOXO-binding partners: it takes two to tango. *Oncogene.* **27:** 2289–2299.
33. Liu, Z. P., Z. Wang, H. Yanagisawa, and E. N. Olson. 2005. Phenotypic modulation of smooth muscle cells through interaction of Foxo4 and myocardin. *Dev. Cell.* **9:** 261–270.
34. Seoane, J., H. V. Le, L. Shen, S. A. Anderson, and J. Massague. 2004. Integration of Smad and forkhead pathways in the control of neuroepithelial and glioblastoma cell proliferation. *Cell.* **117:** 211–223.
35. Li, P., H. Lee, S. Guo, T. G. Unterman, G. Jenster, and W. Bai. 2003. AKT-independent protection of prostate cancer cells from apoptosis mediated through complex formation between the androgen receptor and FKHR. *Mol. Cell. Biol.* **23:** 104–118.
36. Fan, W., T. Yanase, H. Morinaga, T. Okabe, M. Nomura, H. Daitoku, A. Fukamizu, S. Kato, R. Takayanagi, and H. Nawata. 2007. Insulin-like growth factor 1/insulin signaling activates androgen signaling through direct interactions of Foxo1 with androgen receptor. *J. Biol. Chem.* **282:** 7329–7338.
37. Schuur, E. R., A. V. Loktev, M. Sharma, Z. Sun, R. A. Roth, and R. J. Weigel. 2001. Ligand-dependent interaction of estrogen receptor-alpha with members of the forkhead transcription factor family. *J. Biol. Chem.* **276:** 33554–33560.
38. Rudd, M. D., I. Gonzalez-Robayna, I. Hernandez-Gonzalez, N. L. Weigel, W. E. Bingman 3rd, and J. S. Richards. 2007. Constitutively active FOXO1a and a DNA-binding domain mutant exhibit distinct co-regulatory functions to enhance progesterone receptor A activity. *J. Mol. Endocrinol.* **38:** 673–690.